A new satellite-borne neutral wind instrument for thermospheric diagnostics

G. D. Earle,[a] J. H. Klenzing, P. A Roddy, W. A. Macaulay, and M. D. Perdue
William B. Hanson Center for Space Sciences, The University of Texas at Dallas, 800 W. Campbell Road, Richardson, Texas 75083, USA

E. L. Patrick
Honeywell for the Atmospheric Experiments Laboratory, Goddard Space Flight Center, 10210 Greenbelt Road, Greenbelt, Maryland 20771, USA

The bulk motion of the neutral gas at altitudes between about 200 and 600 km is an important factor in predicting the onset of plasma instabilities that are known to distort and/or disrupt high frequency radio communications. These neutral winds have historically been quite difficult to measure, especially from a moving spacecraft. A new space science instrument called the ram wind sensor has been developed to measure the component of the neutral gas velocity that lies along the orbit track of a satellite in low Earth orbit. Laboratory tests of an engineering model of the instrument have been carried out using a supersonic neutral argon beam, in order to validate the measurement concept. The results show that the technique is viable for measurements of neutral flow velocities in future satellite missions. © *2007 American Institute of Physics.* [DOI: 10.1063/1.2813343]

I. INTRODUCTION

In 2008 the US Air Force plans to launch the communication/navigation outage forecast system (C/NOFS) satellite, which is designed to measure a host of geophysical variables relevant to the initiation of equatorial spread F (ESF) irregularities in the ionosphere.[1–3] The ESF instability creates nonlaminar perturbations in the ionospheric plasma density, which in turn produce reflection, refraction, and scintillation of electromagnetic signals propagating in the medium. This process perturbs electromagnetic signals over a broad range of frequencies, so it has consequences that affect both military and civilian systems. Although abundant statistical data exist regarding the onset, duration, and intensity of ESF events, it is currently not possible to accurately predict its occurrence. The goal of the C/NOFS mission is to demonstrate that such prediction is feasible, by linking pseudo real-time data with state of the art geophysical models.

The C/NOFS satellite will be launched into a low inclination elliptical orbit with a perigee near 400 km. The satellite will carry a wide variety of instruments to study the properties of the ionized and neutral gases, as well as the electric and magnetic fields pervading the medium. Most of these instruments have abundant flight heritage, but one, called the neutral wind meter, is a new instrument that has never flown before. Since the bulk flow of the neutral gas is thought to be a key parameter in the onset of ESF, this instrument is of prime importance to the mission.

The University of Texas at Dallas has developed the two neutral wind sensors that comprise the C/NOFS neutral wind meter. One of these sensors is designed to measure the two components of the neutral wind in the plane perpendicular to the satellite's velocity vector. This device uses a differential pressure measurement to infer the arrival angle of the neutral gas relative to the satellite's velocity vector; it has been described in detail by Hanson *et al.*[4] The component of the neutral flow along the orbit track will be measured by a new device called the ram wind sensor (RWS). In this article we describe the RWS and its operating principles, and then show laboratory data from a series of tests conducted in a supersonic neutral jet expansion facility. It will be shown that these data confirm the viability of the measurement technique, provide empirical estimates of the instrument's resolution, and generally validate the performance of the RWS instrument.

II. THE RAM WIND SENSOR

Figure 1 shows a cut-away view of the RWS sensor with the major elements labeled. In flight, the instrument must be mounted on the front surface of the spacecraft such that the plane containing the circular knife-edge aperture is perpendicular to the velocity vector of the satellite (the ram direction). This configuration accomplishes two goals. First, it ensures that the incoming stream of neutral particles enters the aperture free of wake effects from solar panels, antennas, or other satellite surfaces. Second, since the velocity of the satellite is much larger than both the thermal velocity of the ambient gas and any directed component of the geophysical neutral wind in the Earth-fixed frame, this configuration ensures that a supersonic beam of gas will enter the aperture at nearly normal incidence to the aperture plane. The internal structures within the RWS limit the acceptance angle of the incoming gas to a 15° half angle.

At the altitudes of interest the beam of particles that

78, 114501-1
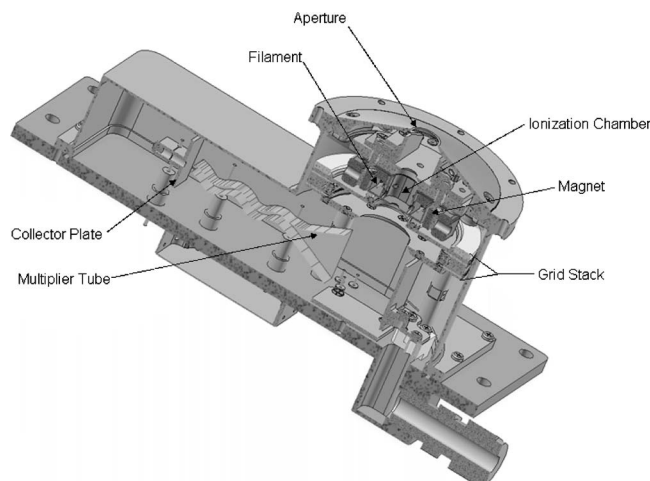
FIG. 1. Cut-away view of the ram wind sensor (RWS), showing the main functional elements.
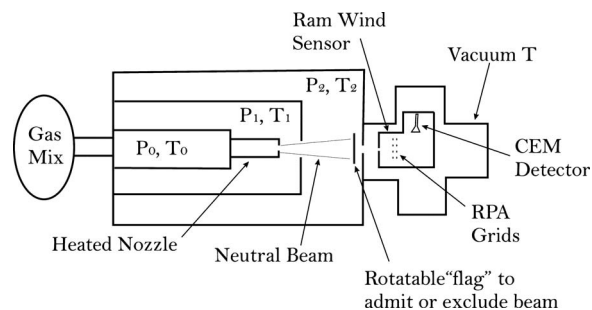

FIG. 2. Basic configuration of the differentially pumped beam expansion chamber used in the validation experiments. High pressures and temperatures within the nozzle lead to supersonic expansion of gas into the vacuum region. The instrument aperture lies on the beam axis, and the rotatable flag can be positioned to block the beam.

enters the aperture will be comprised of neutral particles, positively charged ions, and electrons. The latter two are minor constituents, comprising about 1% of the total flux. However, to correctly analyze the neutral beam it is necessary to remove the ions and electrons from the incoming stream. This is accomplished by placing electrically biased plates inside the RWS near the aperture. As the gas flows past these plates the charged particles are excluded from the beam without significantly perturbing the neutral particle distribution.

The supersonic beam of neutral particles next enters the ionization chamber, where it intersects a beam of electrons that is constrained by a magnetic field that permeates the chamber. The purpose of the electron beam is to ionize a small fraction (about 1 in 10^6) of the neutral particles so that their energy distribution can be measured electronically. The electron beam is produced by a tungsten-rhenium filament housed outside the ionization chamber, and an external magnetic field is aligned with the axis of the beam in order to constrain the electron motion. This is necessary to prevent stray electrons from producing ionization elsewhere in the instrument, which could lead to false signals and increased noise levels in the data.

The momentum of the electrons in the ionizing beam is small compared to that of the incoming neutrals, most of which have a mass near 16 amu at ionospheric altitudes. As a result, the thermal distribution of the ions produced in the beam is essentially the same as that of the incoming neutral beam. A channel electron multiplier (CEM) is used to detect the ions after they have passed through the grid stack (see Fig. 1). The raw data signal is obtained by measuring the current to the collector plate, which is proportional to the number of ions incident on the multiplier tube as a function of the voltage applied to a retarding voltage (RV) grid within the grid stack. The resulting current-voltage (*IV*) characteristic can then be analyzed using the retarding potential analysis technique[5,6] to infer the ram component of the velocity of the incident neutral beam relative to the spacecraft. Since the spacecraft velocity is well known at all times, this measurement can be converted easily into the Earth-fixed frame.

Sensitivity for the RWS instrument is expected to be on the order of 10 m/s in low Earth orbit, and the period of the voltage sweep on the retarding grid is sufficient to provide spatial resolution of a few kilometers. This is more than sufficient for the C/NOFS application, since the numerical models that will utilize the wind measurements have a spatial resolution on the order of 50–100 km. The practical altitude range for the RWS instrument is up to about 600 km in Earth's atmosphere, which covers the regions of interest for the C/NOFS mission. At these altitudes the C/NOFS satellite will encounter neutral wind speeds up to ~600 m/s in the Earth-fixed frame, and temperatures from 1000–1500 K. The validation tests described below involve carrier gas temperatures that cover this range, and velocity resolution to a level that is consistent with C/NOFS mission requirements. In addition to the C/NOFS experiment, the RWS may also prove useful on future planetary missions, such as investigations of the Martian thermosphere.

III. THE NEUTRAL BEAM TEST FACILITY

The Atmospheric Experiment Branch at the Goddard Space Flight Center maintains a three-stage differentially pumped neutral beam system capable of producing supersonic fluxes of various neutral gases. It uses a free jet expansion geometry[7] to accelerate a minority species seed gas embedded in a carrier gas of lighter molecules. A schematic diagram showing the major components of the system is shown in Fig. 2.

The figure shows the gas mix volume on the left, along with three vacuum pumped stages which ensure that the pressure continually decreases as the gas mixture flows toward the target. At the far end of the chamber (about 2 m from the source) is a flange that connects to a vacuum-T structure that houses the RWS instrument and electronics. Mounted directly in front of the RWS is a metal plate that can be rotated in front of the aperture, thereby blocking the directed neutral beam without sealing the opening between the instrument and the beam chamber. This device is called the flag due to its similarity to the flag on a typical household mailbox.

The gas mix at the far left contains the seed and carrier gases in a ratio of 1 part seed gas to 99 parts carrier. In our experiments argon is used as the seed, and hydrogen as the
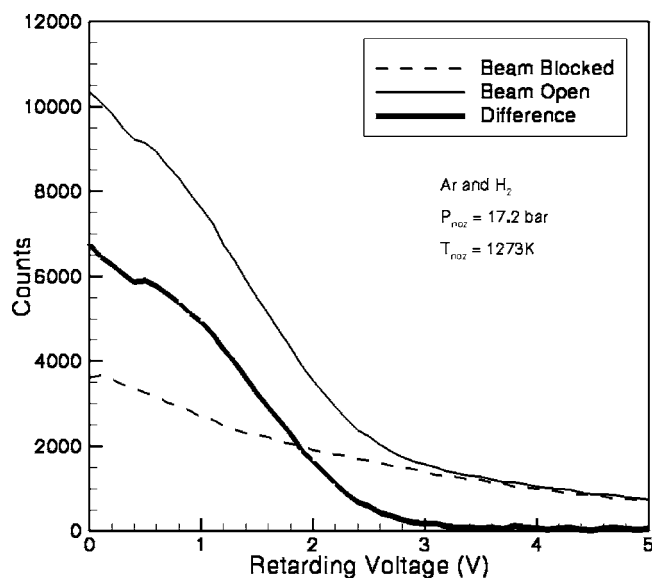
FIG. 3. Examples of current measured as a function of retarding voltage. The signal of interest is the differential current obtained by subtracting the thermal flux current (beam blocked) from the net beam current (beam open).
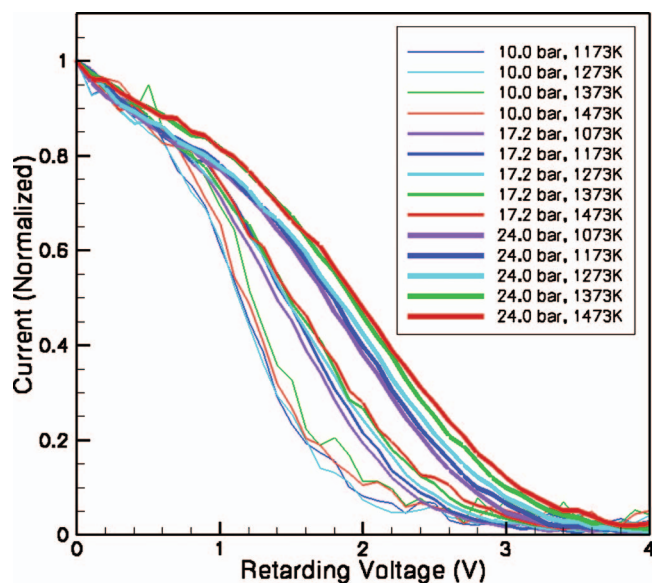

FIG. 4. (Color) Differential current (as defined in Fig. 3) vs retarding voltage for all test cases. The inset box shows the nozzle pressures and temperatures for each case.

carrier gas. The gas mixture is admitted to the high pressure nozzle system and maintained at pressures ranging from 1.0 to 2.4 MPa during normal operation. The nozzle is a silicon carbide tube that is heated to temperatures of 1100–1500 K to create the free jet expansion.[8] During operation the seed gas is accelerated by the jet expansion to velocities close to the thermal velocity of the heated carrier gas.[7] The expanding beam of neutral gas has a relatively high concentration of the heavier seed gas near the center of the beam, due to the larger transverse velocity of the lighter carrier gas. As a result, a neutral beam of the seed gas is created that has a very large directed velocity along the chamber's axis.

IV. DATA PRESENTATION

Figure 3 shows a typical example of the RWS measurements during the experiment. The ordinate shows the counts obtained from the detector, and the abscissa shows the retarding voltage applied to the grid. There are three curves shown in the figure; the light solid curve shows the average of five retarding voltage sweeps with the flag in the open position, and the dashed curve shows a similar average with the flag closed to block the beam. In the latter case the neutral gas molecules entering the RWS aperture have undergone many collisions with the grounded, room temperature walls of the chamber system. This curve therefore represents a thermal noise characteristic, while the data taken with the flag open correspond to the beam signature plus the noise background. Of interest here is the difference between these two signals; this differential *IV* curve is represented by the dark solid curve in Fig. 3.

The validation experiments involve collecting current-voltage (*IV*) characteristics for a variety of different nozzle conditions. Difference signals such as the dark solid line shown in Fig. 3 are obtained at three different nozzle pressures and at a variety of temperatures for each pressure. In all cases five curves are collected at each setting, and the difference signals between the flag-open and flag-closed cases are used in subsequent processing. The average of five retarding voltage sweeps is used in all cases because the total neutral flux from the system is far less than what the instrument will encounter during spaceflight, therefore the signal to noise ratio (SNR) is lower in the laboratory environment. Averaging five data curves for each case helps to increase the SNR by averaging out some of the random variations.

The pressure in the outermost vacuum chamber during each experiment (and within the RWS instrument) is held at a constant level of ~50 μPa, while the pressure within the silicon carbide nozzle varies from 1.0 to 2.4 MPa. The only other controllable variable capable of affecting the neutral beam velocity distribution is the nozzle temperature, which varies over a range from ~1100 to 1500 K (900–1200 C).

The differential *IV* curves for each case are normalized and plotted together in Fig. 4 to allow easy comparison. It is immediately apparent in the figure that the curves segregate into three groups, corresponding to the three different nozzle pressures tested. Furthermore, the slope of the *IV* characteristic generally varies in a systematic way with increasing nozzle temperature, at least for the two higher pressure runs, which have the largest SNR values. These features are consistent with theoretical expectations, as shown in the next section.

V. DATA ANALYSIS

The differential *IV* characteristics are analyzed using a Levenberg-Marquardt[9] nonlinear fitting routine to solve for the velocity of the argon-hydrogen neutral gas mix known to comprise the beam. The form of the function used in these fits is given by Knudsen[6] as
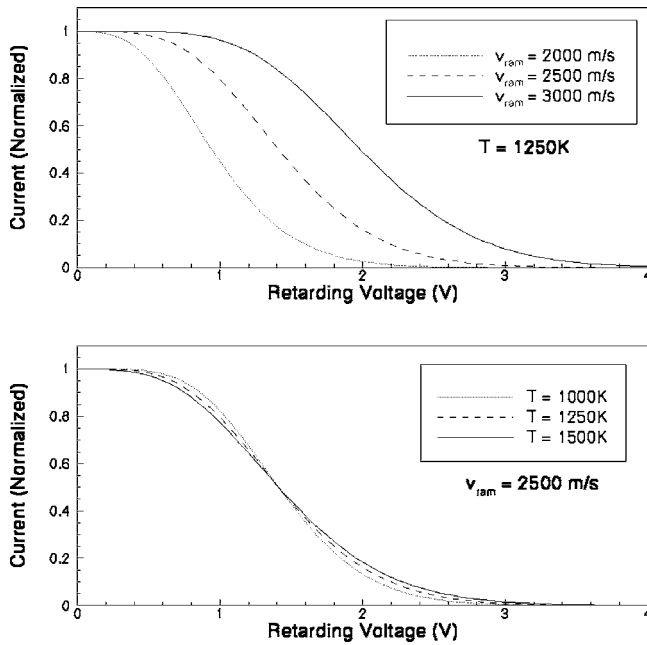
FIG. 5. Theoretical retarding potential analysis *IV* curves for a flowing gas with constant temperature (top) and constant velocity (bottom).

$$N = \sum_i f_i \left[\tfrac{1}{2} + \tfrac{1}{2}\, \mathrm{erf}(\kappa_i) + \frac{\exp(-\kappa_i^2)}{2\sqrt{\pi}a_i} \right], \tag{1}$$

$$\kappa_i = \frac{v\cos\theta}{\sqrt{2KT_i/M_i}} - \sqrt{\frac{eV}{KT_i}}, \tag{2}$$

$$a_i = \frac{v\cos\theta}{\alpha_i}, \tag{3}$$

where f_i is the fractional composition of each component gas, V is the retarding potential, and θ is the angle between the incoming beam and the aperture plane. The other parameters in Eqs. (1)–(3) are N the ion density, v the velocity of the beam, M and T the mass and temperature of the ionized constituents, α_i the ion thermal speed, and Boltzman's constant K. The total current is then given by

$$I = NevA, \tag{4}$$

where e is the fundamental unit of electronic charge and A is the collecting area.

Figure 5 illustrates the theoretically expected[5,6] effects of varying the temperature and velocity of the neutral gas in a supersonic beam expansion geometry. The curves show the results of using Eqs. (1)–(4) to calculate the current for a beam comprised of pure argon as the velocity and temperature vary. In the top panel the temperature is held at 1250 K and the velocity is varied from 2000 to 3000 m/s. The result is that the *IV* curve shape is unchanged, but the curve slips to the right corresponding to the larger voltages required to retard ions having higher velocities. The bottom panel shows the simulated results for an argon beam with a constant velocity of 2500 m/s, but with temperature varying from 1000 to 1500 K. As expected, variation of the temperature changes the shape of the distribution, with no net offset along the energy (retarding voltage) axis.
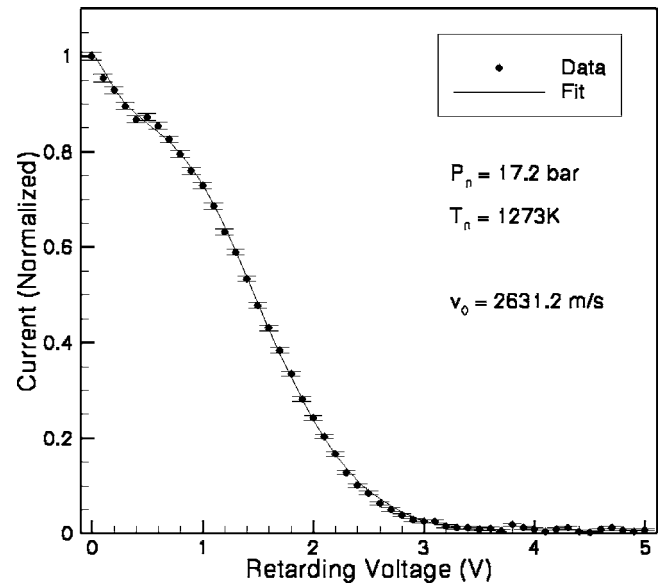

FIG. 6. Example of a nonlinear fit to a typical differential *IV* curve using Eqs. (1)–(4). The nozzle temperature and pressure are given in the inset text, as is the velocity inferred from the fit to Eq. (1).

In light of the calculated results in Fig. 5 the qualitative behavior shown in Fig. 4 seems quite sensible. The segregation of the *IV* curves into three distinct groups satisfies the intuitive expectation that the velocity of the neutral beam should depend sensitively on the nozzle pressure. Since the beam comprises both hydrogen and argon the general shape of the curve is consistent with two overlapping functions of the type shown in Fig. 5; if both hydrogen and argon have the same directed velocity then less energy is required to retard the hydrogen, giving rise to the bump seen at low retarding voltages. The portion of the curve corresponding to argon energies is the broader distribution in which the current is reduced by about a factor of two at retarding voltages between one and two volts. The contribution of hydrogen to the total current at this energy is essentially negligible, as may be verified using Eqs. (1)–(4).

Figure 6 shows the result of applying the Levenberg-Marquardt[9] nonlinear fitting algorithm to a typical differential *IV* curve. The symbols show the normalized average differential *IV* points, with the error bars indicative of the spread in the five individual runs used in each average. The solid line shows the fit, which in this case has a χ^2 value of 4.09×10^{-6}. All of the fits to our differential *IV* curves have χ^2 less than 2×10^{-5}, which strongly supports the veracity of the analysis.

The summary results of performing the fitting procedure on all data runs are shown in Fig. 7. This plot shows the velocity values obtained from the fits as a function of the nozzle pressure. The spread of data points at each pressure is associated with the uncertainty due to the broad range of nozzle temperatures. It is noteworthy that the largest dispersion in the fitted velocities is only about 4%, despite the 20% temperature variations imposed at the nozzle. This provides some assurance that the instrument is capable of resolving the velocity of the neutral beam over a relatively wide temperature range, such as it will encounter during spaceflight.
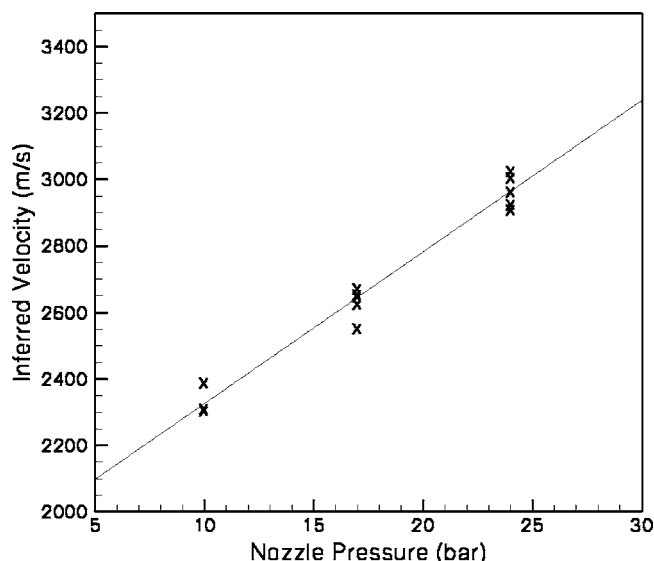
FIG. 7. Variation of the velocity inferred from the fits to each of the differential *IV* curves shown in Figure 4. The spreads correspond to variations in the nozzle temperature at each pressure.

VI. DISCUSSION

The validation measurements shown in Fig. 7 indicate that there is a linear relationship between the nozzle pressure and the flow speed of the expanding gas jet. In a qualitative sense this linear variation is straightforward to explain, because the process by which the seed gas (Ar) is accelerated to velocities near the thermal velocity of the carrier gas (H_2) is collisional. For ideal gases, higher pressures within the nozzle correspond to higher number densities, so the collisional coupling between the two species should increase as the pressure increases. Since the thermal velocity of the H_2 is a function of the nozzle temperature, it is also likely that the Ar beam velocity depends on this parameter, though perhaps in a much weaker sense.

The detailed theory describing the free jet expansion of a gas mixture from a high pressure, heated nozzle aperture into an adjacent vacuum region is quite complex. In the physical setup described here the situation is further complicated by the multistage differentially pumped vacuum system, the presence of a skimmer to help collimate the expanding beam along the expansion axis, and by the mixture of two gases with very different masses (which may lead to slip-flow conditions downstream of the nozzle).

A review of the physics associated with such supersonic expansions is presented by Miller.[7] As the gas flows out of the nozzle a boundary shock region called the Mach disk is formed many aperture diameters downstream from the nozzle outlet. For the conditions prevailing during the validation study described here the RWS instrument aperture lies well upstream of this Mach disk shock, in a region termed the zone of silence. Within this zone the Mach number of the flowing beam is much greater than unity, and the velocity and various other flow parameters describing the beam can be expressed as functions of the local Mach number. Unfortunately, there is no analytic solution for the variation of Mach number as a function of nozzle pressure and temperature corresponding to our physical configuration, since this requires explicit solution of the Boltzmann equation in the noncontinuum flow transition regime for the specific geometry of interest.

Despite the complexities of the theory and the nonanalytic nature of the functional dependencies, two general characteristics of free jet expansion geometries are theoretically justified and empirically well documented. First, the high pressure within the nozzle relative to the background pressure ensures that the carrier gas (H_2) exits the nozzle supersonically. Second, the smaller diffusion velocity of the seed gas (Ar) perpendicular to the beam axis guarantees that its relative density near the center of the expanding axisymmetric beam will be substantially higher than that of the initial mixing ratio. Thus the physical configuration of the expansion chamber is appropriate for our validation experiment, and qualitatively consistent with the form of the characteristic curves we observe.

Given the theoretical complications, the most feasible approach for validating the results shown in Fig. 7 is comparison with an independent empirical technique, preferably one associated with a very similar physical apparatus. Patrick[8] reports such measurements in the same chamber for the same relative argon-hydrogen gas mixture at temperatures near 1200 and 1500 K. In these experiments a time-of-flight detection technique revealed linear variations of metastable argon atoms over the same pressure range investigated in our validation experiments. It is noteworthy that the slopes of the velocity versus pressure curves obtained in these previous experiments are different from those reported here, with higher velocities measured at all pressures tested. However, this is perhaps not too surprising given that the experiments described by Patrick[8] involve a somewhat different nozzle and skimmer configuration. Despite these differences, these earlier independent measurements confirm the linear behavior of the Ar beam velocity as a function of nozzle pressure, and provide anecdotal confirmation of the behavior shown in Fig. 7.

Since it is not possible to configure both the time-of-flight measurement apparatus and the RWS instrument in the chamber simultaneously, we cannot validate the absolute accuracy of the RWS measurements using a simultaneous independent measurement. However, it is possible to draw conclusions about the resolution of the technique based on the measurements presented here. This in itself is very useful for validating the flight instrument, since the variations of the measured parameters are often quantities of significant interest in the space environment. For example, in large-scale gravity wave studies the wavelength and amplitude of the wave fluctuations are the quantities of interest, and the velocity of the background flow is less important. In studying these waves it is therefore vital to obtain good resolution of fluctuation levels as the satellite cuts through the wave fronts, but it is less important to measure the steady state drift.

The resolution of the RWS instrument can be estimated by starting with the noise level of the current sensing electronics, which can be used in conjunction with Eqs. (1)–(4) to determine the degree of uncertainty associated with the

voltages in the *IV* characteristics. The relationship between the kinetic energy of the particles in the beam and the retarding potential required to repel them is

$$\frac{1}{2}mv^2 = e\phi, \tag{5}$$

where v is the velocity of the particles normal to the aperture, m is their mass, e is the charge, and ϕ is the retarding potential. In an average sense we then obtain

$$\delta v = \frac{e}{m\langle v \rangle}\delta\phi, \tag{6}$$

where $\langle v \rangle$ is the average velocity. The uncertainty δv due to the inherent instrument resolution of the collected current is estimated by applying Eq. (6) to the *IV* curves at the point where the current has its average value. In other words, we find the $\delta\phi$ corresponding to the uncertainty in the value at the middle of the current range in the *IV* curve, and then use Eq. (6) to determine the resolution δv. Using this procedure with the dataset from the lab experiments leads to velocity errors on the order of 4 m/s. In the spaceflight environment the composition of the neutrals is predominantly monatomic oxygen, but the flux levels are orders of magnitude higher than those that can be achieved in the lab. Furthermore, the average velocity of the incoming particles in spaceflight is essentially the orbital speed of the spacecraft, about 8000 m/s. The combination of these factors reduces the uncertainty in the flight environment significantly, to values far less than the uncertainty due to alignment errors between the aperture normal and the velocity vector of the satellite.

Uncertainties associated with neutral gas temperatures may be considered with reference to Figs. 4 and 5. Comparison of the measured data (Fig. 4) with the idealized theoretical curves (Fig. 5) shows that the slopes of the measured curves do not vary in strict accordance with the theoretical expectations. The reason for this is that the equations describing the theoretical curves [Eqs. (1)–(3)] apply to the idealized case in which the grids have zero thickness and produce potential fields that are perfectly uniform. In any real instrument the grids are non-uniform, and in many cases are woven from very thin wires (similar to a window screen). Thus, the real potential fields are distorted relative to the ideal case, so the grids have a weak lensing effect on the particles. This effect is largest for particles with energies near the instantaneous potential of the grid, which results in a distortion of the current-voltage characteristic.

It is also noteworthy that the behavior of the data curves shown in Fig. 4 is not consistent at the lowest nozzle pressures, since some of the curves intersect. This is attributed to the small SNR at the low particle flux levels associated with these nozzle pressures. As stated earlier, this effect will not be a factor during the C/NOFS mission because the neutral particle flux into the instrument during flight will be much larger than that produced in the laboratory environment. This is in part because of the very high velocities associated with satellites in low Earth orbit, but in practice it is also very difficult to produce directed flows of neutral gas with high beam densities in a space-level vacuum environment. Thus, the SNR levels in flight will exceed those in the laboratory tests described here, by factors on the order of 100.

The data presented in Fig. 7 imply that errors in the velocity measurements due to temperature related effects are on the order of ±60 m/s over the range of temperatures expected in spaceflight. This error is larger than both the inherent error from electronic uncertainty and the error due to satellite attitude (aperture pointing) variations. If an independent measurement of neutral temperature is available, or if future numerical studies show that it is possible to estimate simultaneously the neutral temperature using the *IV* curves, then it may be possible to remove the temperature variation during data processing.

VII. CONCLUSION

Laboratory test results confirm that the RWS instrument is capable of measuring the speed of a neutral gas flowing normal to the plane of the ram-facing aperture. The fits to the average *IV* curves from a series of experiments carried out with different forcing conditions at the nozzle match the variations expected, and provide velocity estimates that are reasonable for the specific test conditions. In flight conditions the RWS instrument will encounter monatomic oxygen as the dominant neutral gas constituent. Model values of the neutral temperatures[10] at the altitudes of interest (200–600 km) range from approximately 1100 to 1500 K, which is in the same range as the nozzle temperatures tested and reported here. The laboratory results show that the resolution of relative speed variations is about ±60 m/s, and that this error arises mainly from uncertainties in the neutral gas temperature. The results of these laboratory tests confirm the validity of the general measurement approach inherent in the RWS technique.

It is known that absolute velocity estimates inferred from the retarding potential analysis technique are subject to systematic errors as large as 180 m/s for spaceflight conditions,[11] due strictly to the effects of the nonideal biased grids on the distribution function of the particles. These effects include incomplete shielding of grid potentials, finite grid thickness, and lensing effects as particles pass through the grids. The grid effects are therefore more significant sources of error than the uncertainties related to either electronic resolution or temperature effects. As a final comment, we note that sophisticated numerical simulations of the effects of nonideal grids on flowing Maxwellian particle distributions are currently nearing completion at our institution. These results should provide for significant improvement in the ability to compensate for systematic errors inherent in the practical application of the retarding potential analysis technique.

[1] R. F. Woodman and C. La Hoz, J. Geophys. Res. **81**, 5447 (1976).
[2] B. G. Fejer, J. Atmos. Sol.-Terr. Phys. **59**, 1465 (1997).
[3] D. L. Hysell, J. Atmos. Sol.-Terr. Phys. **62**, 1037 (2000).
[4] W. B. Hanson, U. Ponzi, C. Arduini, and M. Di Ruscio, J. Astronaut. Sci. **40**, 429 (1992).

[5] E. C. Whipple, Proc. IRE **47**, 2023 (1959).

[6] W. C. Knudsen, J. Geophys. Res. **71**, 4669 (1966).

[7] D. R. Miller, *Atomic and Molecular Beam Methods*, edited by G. Scoles (Oxford University Press, New York, 1988), Vol. 1.

[8] E. L. Patrick, Rev. Sci. Instrum. **77** (2006).

[9] D. W. Marquardt, J. Soc. Ind. Appl. Math. **11**, 431 (1963).

[10] M. C. Kelley, *The Earth's Ionosphere* (Academic, San Diego, CA, 1989).

[11] C. K. Chao, S.-Y. Su, and H. C. Yeh, Adv. Space Res. **32**, 2361 (2003).